Lawrence Berkeley Laboratory
UNIVERSITY OF CALIFORNIA

Materials & Molecular Research Division

Submitted to Oxidation of Metals

THE FORMATION OF SOLID SOLUTION OXIDES DURING INTERNAL OXIDATION

D.P. Whittle, F. Gesmundo, B.D. Bastow, and G.C. Wood

September 1980

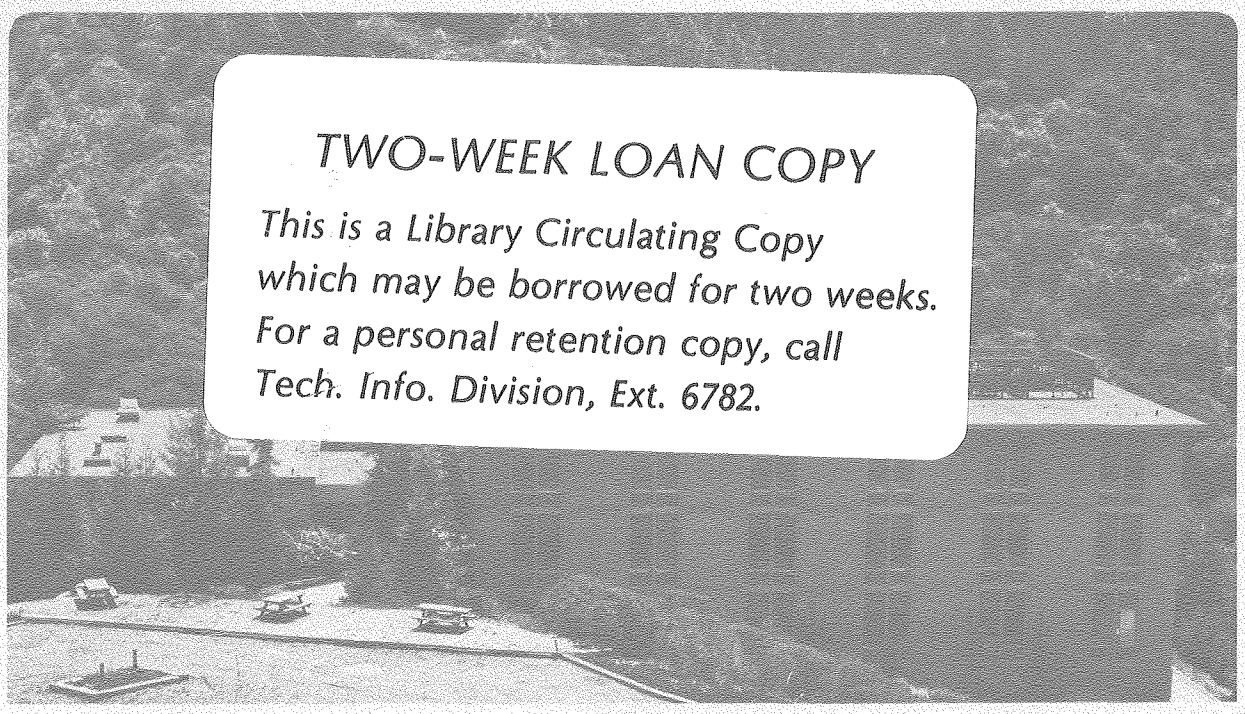

Prepared for the U.S. Department of Energy under Contract W-7405-ENG-48

DISCLAIMER

LBL-11496

THE FORMATION OF SOLID SOLUTION OXIDES DURING INTERNAL OXIDATION

D.P. Whittle
Lawrence Berkeley Laboratory, University of California,
Berkeley, California 94720 USA

F. Gesmundo
Centro Studi di Chimica Applicata, Consiglio Nazionale delle
Ricerche, Genova, Italy

B.D. Bastow
British Nuclear Fuels, Ltd., Windscale Works, Seascale, Cumbria,
England

G.C. Wood
Corrosion and Protection Center, UMIST, Manchester M60 IQd,
England

Abstract: The diffusion processes occurring when binary alloys react with oxygen to form an oxide that contains both alloy components in solid solution, either exclusively as internal oxide or in combination with a surface scale, have been analyzed and compared with experimental results for Fe-Mn and Ni-Co alloys. The experimental results available for the Fe-Mn system were obtained under conditions of exclusive internal oxidation, and good agreement was obtained between calculated and experimental results. In the Ni-Co system, a surface scale and a zone of internal oxidation develop. Agreement between calculated and experimental depths of internal penetration is acceptable if the diffusivity of oxygen in the alloy is 3.8×10^{-6} cm^2/s at 1100°C. Agreement between calculated and experimental concentration profiles is not very good.

Introduction

A theoretical description of the internal oxidation of binary alloys for those systems where the internal oxide precipitates consist of a solid solution of the oxides of both alloy components has recently been developed by Whittle et al. [1]. This general treatment shows that, in contrast to systems where the internal oxide contains only one alloy component, the fraction of internal oxide precipitates within the internal oxidation zone falls off rapidly with distance into the alloy and there is no sharp delineation of the front of internal oxidation. In addition, the composition of the oxide precipitates varies throughout the internal oxidation zone, with an increasing concentration of the more stable oxide component at increasing depths below the surface.

The importance of the thermodynamic relationships of the alloy-oxygen system and the kinetic parameters was demonstrated; namely, the diffusion of oxygen into the alloy and the overall growth rate of the surface scale (also consisting of a solid solution of the oxides of the alloy components) when this forms simultaneously with a zone of internal oxidation. A theoretical analysis of the growth of solid solution surface scales was presented earlier [2]. The present paper compares the theoretical predictions of the internal oxidation model with the very limited experimental data available: Both the thickness of the internal oxidation zone and the variation of precipitated oxide and alloy

compositions throughout the internal oxidation zone can be compared. Two distinctive types of system are considered:

(i) Fe-Mn alloys [3] oxidized in the temperature range 950-1350°C in a H_2-H_2O atmosphere of insufficient oxygen potential, to form a surface scale representing a system in which there is exclusive internal oxidation.

(ii) Ni-Co alloys [4] oxidized in oxygen at 1100-1200°C, representative of a system in which the component with the higher affinity for oxygen (Co) is the faster diffusing species in the solid solution oxide.

Theoretical Description

If both alloy (AB with B representing the component with the higher oxygen affinity) and oxide (AO-BO) systems are thermodynamically ideal, then the local equilibrium relationships between B in the alloy or BO in the oxide phase with the activity of oxygen dissolved in the alloy can be established.

$$N_B = \frac{\Omega/\beta a_O - 1}{\Omega - 1} \tag{1}$$

$$N_{BO} = \frac{\Omega - \beta a_O}{\Omega - 1} \tag{2}$$

where

$$\Omega = \exp\left[-\frac{1}{RT}\left(\Delta G^o_{BO} - \Delta G^o_{AO}\right)\right] \tag{3}$$

and

$$\beta = \exp\left[-\frac{1}{RT}\Delta G^o_{BO}\right] \tag{4}$$

Combining Eqs. (1) and (2) also gives the local equilibrium condition between B in the alloy phase and BO in the oxide phase:

$$N_{BO} = \frac{1}{1 + \frac{1}{\Omega}\left(\frac{1}{N_B} - 1\right)} \tag{5}$$

In the subscale zone, the total amount of oxygen per mole of alloy is $N_O + r$, where r is the ratio of the number of moles of precipitated oxide to the number of moles of metallic components of the alloy. Thus, assuming that the amount of precipitated oxide is small, so that volume changes and blockage of the diffusion by the precipitate can be neglected, the rate of change of the total amount of oxygen per mole of alloy at position x is given by

$$\frac{\partial}{\partial t}(N_O + r) = D_O \frac{\partial^2 N_O}{\partial x^2} \qquad X_1 < x < X_2 \tag{6}$$

which can be rearranged to give

$$\frac{\partial N_O}{\partial t} = \frac{N_O}{1 + \frac{\partial r}{\partial N_O}} \frac{\partial^2 N_O}{\partial x^2} \qquad X_1 < x < X_2 \tag{7}$$

X_1 and X_2 are the positions of the surface scale/alloy and subscale/alloy interfaces respectively, measured from the original alloy surface.

If there is no countercurrent diffusion of B towards the alloy surface--a condition anticipated for the systems being considered, as will be demonstrated later--then there will be no overall change in composition in the internal oxide zone, but only a repartitioning of B between alloy and internal oxide. Thus, the mass fraction, f, of precipitated oxide within the internal oxidation zone is given by the lever rule

$$f = \frac{N_B - N_B^O}{N_B - N_{BO}} \tag{8}$$

where N_B^O is the mole fraction of B in the original alloy. r, given earlier, and f are related through

$$r = \frac{f}{1 - f} \tag{9}$$

and thus

$$r = \frac{N_B - N_B^O}{N_B^O - N_{BO}} \tag{10}$$

Furthermore, using Eqs. (1) and (2), r can be expressed as a function of the oxygen activity a_O or, if it can be assumed that

oxygen dissolution in the alloys follows Henry's law, then r can be expressed as a function of N_0, the atomic fraction of dissolved oxygen.

$$r = \frac{\Omega\,/\beta\gamma_0^0 N_0 - 1 - N_B^0(\Omega - 1)}{(\Omega-1)N_B^0 - \Omega + \beta\gamma_0^0 N_0} \tag{11}$$

This then is the relationship required to substitute in Eq. (7) for $\partial r/\partial N_0$

$$\frac{\partial N_0}{\partial t} = D_0^{eff}\,\frac{\partial^2 N_0}{\partial x^2} \qquad X_1 < x < X_2 \tag{12}$$

with

$$D^{eff} = \frac{D_0}{1 + \partial r/\partial N_0} \qquad X_1 < x < X_2 \tag{13}$$

and, as was indicated earlier [1], $\partial r/\partial N_0$ can be taken as constant for these types of systems when Eq. (12) has a normal error function solution:

$$N_0 = N_0^I - (N_0^I - N_0^{II})\,\frac{\operatorname{erfc}\dfrac{x}{2\sqrt{D_0^{eff}\,t}} - \operatorname{erfc}\dfrac{X_1}{2\sqrt{D_0^{eff}\,t}}}{\operatorname{erfc}\dfrac{X_2}{2\sqrt{D_0^{eff}\,t}} - \operatorname{erfc}\dfrac{X_1}{2\sqrt{D_0^{eff}\,t}}} \qquad X_1 < x < X_2 \tag{14}$$

Diffusion of oxygen ahead of the internal oxidation zone, $x > X_2$, also follows Eq. (12), but with D_0 replacing D_0^{eff}, giving

$$N_0 = N_0^{II} \frac{\operatorname{erfc} \dfrac{x}{2\sqrt{D_0 t}}}{\operatorname{erfc} \dfrac{X_2}{2\sqrt{D_0 t}}} \tag{15}$$

N_0^I and N_0^{II} are the atomic fractions of dissolved oxygen at the surface scale/subscale and subscale/alloy interfaces, respectively. Equating the oxygen fluxes on either side of the interface, $x = X_2$, since there is no internal oxide formation there, gives a transcendental equation for γ_2

$$\frac{N_0^I - N_0^{II}}{N_0^I} \sqrt{1 + \frac{\partial r}{\partial N_0}} = \exp\left[\frac{\gamma_2^2 \, \partial r/\partial N_0}{1 + \partial r/\partial N_0}\right] \frac{\operatorname{erfc} \gamma_1 - \operatorname{erfc} \partial_2}{\operatorname{erfc} \gamma_2 / \sqrt{1 + \partial r/\partial N_0}} \tag{16}$$

where

$$\gamma_1 = \frac{X_1}{2\sqrt{D_0^{eff} t}} = \sqrt{\frac{K_1}{D_0^{eff} t}} \quad \text{and} \quad \gamma_2 = \frac{X_2}{2\sqrt{D_0^{eff} t}} = \sqrt{\frac{K_2}{D_0^{eff} t}} \tag{17}$$

K_1 and K_2 are parabolic rate constants describing the displacements of the surface scale/subscale and subscale/alloy interfaces with time, respectively.

Thus, solution of Eq. (16) gives γ_2 and K_2, the parabolic rate constant for the penetration of the front of internal oxidation, and solution of Eq. (14) gives the profile of dissolved oxygen through the internal oxide zone. Use of Eqs. (1), (2), and (8) then permit the composition of the alloy, the composition of the internal oxide, and the fraction of the internal oxide, respectively, to be calculated throughout the subscale region.

In cases where no external surface scale develops, Eqs. (14) and hence Eq. (16) are then modified to

$$N_O = N_O^I - (N_O^I - N_O^{II}) \frac{\operatorname{erf} \dfrac{x}{2\sqrt{D_O^{eff} t}}}{\operatorname{erf} \dfrac{X_2}{2\sqrt{D_O^{eff} t}}} \qquad 0 < x < X_2 \tag{18}$$

and

$$\frac{N_O^I - N_O^{II}}{N_O^{II}} \sqrt{1 + \frac{\partial r}{\partial N_O}} = \exp\left[\frac{\gamma_2^2 \, \partial r/\partial N_O}{1 + \partial r/\partial N_O}\right] \frac{\operatorname{erfc} \gamma_2}{\operatorname{erfc} \gamma_2 / \sqrt{1 + \partial r/\partial N_O}} \tag{19}$$

respectively

Solution of Eqs. (16) or (18) requires the values of N_O^I and N_O^{II}, the atomic fractions of dissolved oxygen at the outer and inner interface of the internal oxidation zone, respectively. Under the earlier assumption, N_O^{II} can be determined since, in the

absence of any counterdiffusion, N_B at $x = X_2$ will be equal to the bulk mole fraction of B in the alloy N_B^o, and N_B and N_O^{II} and thus related through the alloy-oxygen thermodynamics. In the absence of a surface scale, N_O^I will be fixed by the oxygen activity in the atmosphere, and this can be calculated providing the activity coefficient of Henry's law is known. When a surface scale is present the situation is less clear, although it may be possible to calculate N_O^I when the more stable cation has the slower diffusivity in the surface scale [1]. When the more stable cation has the faster diffusivity in the surface scale, as in the Ni-Co system, this is not possible: The value of N_O^I or r_{max} or f_{max}, the maximum fraction of subscale, cannot be determined a priori.

Fe-Mn System

Swisher [3] oxidized Fe-1 wt. percent Mn in a H_2-16.67 percent H_2O ($P_{H_2O}/P_{H_2} = 0.2$) mixture in the temperature range 950-1350°C, analyzing the results on the basis of a linear oxygen concentration gradient, which introduces a considerable approximation.

According to Swisher and Turkdogan [5], the diffusivity of oxygen at 1350°C is 1.9×10^{-5} cm^2/s, while the diffusivity of Mn in the alloy at the same temperature is 6.3×10^{-10} cm^2/s [6]. Thus, the assumption that there is no counterdiffusion of Mn during internal oxidation is entirely valid. Both Fe-Mn [7,8]

and FeO-MnO [9] can be considered as thermodynamically ideal, with the following free-energy changes taken from Kubachewski et al. [10].

$$Mn(s) + 1/2\ O_2(g) = MnO(s) \qquad \Delta G^o = -91{,}950 + 17.4\ T \text{ cals.}$$

$$Fe(s) + 1/1\ O_2(g) = FeO(s) \qquad \Delta G^o = -61{,}050 + 14.95\ T \text{ cals.}$$

Thus, the values of the thermodynamic constants, Ω, and β, defined earlier, can be calculated. These are given in Table I for a temperature of 1350°C.

The dissolution of oxygen in Fe from H_2/H_2O mixtures was represented by [3]

$$H_2O(g) = H_2(g) + \underline{O}$$

where $\underline{O}$ denotes oxygen in solution and the equilibrium constant for this reaction is given as [5]

$$\log \frac{p_{H_2}[\%O]}{p_{H_2O}} = -\frac{4050}{T} - 0.06 \tag{20}$$

Thus, using Eq. (20), the solubility of oxygen in Fe at 1350°C is calculated, along with the partial pressure or activity of oxygen in the H_2O/H_2 mixture, using the free energy for the reaction [10]:

$$H_2O(g) = H_2(g) + 1/2\ O_2(g) \qquad \Delta G^o = 57250 - 4.48T \log T + 2.21T$$

Hence, the Henrian activity coefficient for oxygen solution in Fe is obtained. These data are included in Table I. Using these data, the parameters included in Table II have then been calculated from the equations presented earlier.

The parameter γ_2 is a measure of the rate of propagation of the internal oxidation front into the alloy as defined by Eq. (17). This can be converted to the measured parameter, α^2, as defined by Swisher [3], where

$$X_2^2 = \alpha^2 t$$

and

$$\alpha^2 = 4 \gamma_2^2 D_0^{eff} = 4 \gamma_2^2 D_0/(1 + \partial r/\partial N_0).$$

Thus, the present analysis gives a value of α^2 of 4.6×10^{-7} cm^2/s, which is somewhat greater than that measured experimentally, 7.4×10^{-8} cm^2/s, or computed from the theoretical analysis of Swisher, 1×10^{-7} cm^2/s. However, there are various reasons for this.

Figure 1 shows the variation of the fraction of oxide precipitate, the composition of the internal oxide particles, and the composition of the alloy as a function of dimensionless distance within the internal oxidation zone. The fraction of internal oxide precipitate is only 0.012 (1.2 percent) at the surface of the alloy—its maximum value—and falls off rather rapidly through the internal oxide zone, decreasing to about 0.004 half-way across it. This means that it would be very difficult to observe the actual

precipitation front with an optical microscope. The author comments, "The interface was well-defined at the lower temperatures but somewhat irregular at 1350°C." As a result, the measured value of α^2 probably represents a considerable underestimate of the depth of penetration of the internal oxide front. Indeed, in view of the rapidly decreasing fractions of precipitated oxide, a better indication of the depth of internal oxidation can be obtained from Swisher's measurement of the concentration profile of Mn within the alloy after internal oxidation. After 1 h exposure at 1350°C to the $H_2O/H_2(0.2)$ mixture, a depletion of Mn to a depth of approximately 2×10^{-2} cm below the surface is measured. This corresponds to a value of α^2 of 1.1×10^{-7} cm^2/s, which is somewhat closer to that calculated using the present analysis. Again, some underestimation is anticipated since the Mn concentration profile is very flat near to the internal oxidation front.

Perhaps a better test of the current analysis is to compare the calculated and measured Mn-concentration profiles. Unfortunately, no measurements of the fraction of internal oxide particles or their composition are available. However, the measured Mn-concentration profile in the internal oxidation zone is included in Fig. 1, which has been plotted as a function of dimensionless distance to nullify uncertainties in the precise depth of the internal oxidation front. The agreement in shape and in absolute value is considered an acceptable test of the current analysis. The concentration profile

calculated according to Swisher's analysis is also included but, due to the assumptions made, there was a physically unlikely discontinuity at the alloy/internal oxide interface.

Figure 2 compares the internal oxide composition, expressed as the ratio of mole fractions of oxygen to manganese in the oxide, as a function of fractional distance into the subscale, calculated according to the present analysis and that of Swisher. The latter tends to underestimate the Mn concentration in the internal oxide particles.

Ni-Co System

As in the Fe-Mn system, both Ni-Co and NiO-CoO solid solutions approximate very closely to ideal behavior, with the following free-energy changes taken from Kubaschewski et al. [10]:

$$Co(s) + 1/2\ O_2(g) = CoO(s) \qquad \Delta G^O = -55{,}900 + 16.9\ T \text{ cal.}$$

$$Ni(s) + 1/2\ O_2(g) = NiO(s) \qquad \Delta G^O = -58{,}450 + 23.55\ T \text{ cal.}$$

Thus, the thermodynamic constants Ω and β can be calculated, and their values at 1100°C are given in Table III. These parameters also permit the calculation of the Ni-Co-p_{O_2} diagram, and this is shown in Fig. 3.

Ferguson and Stott [4] have studied the oxidation behavior of Ni-Co alloys in the temperature range 1000-1200°C in 1 atm oxygen.

Under these conditions, a surface scale of the solid solution NiO-CoO grows essentially at a parabolic rate; but, in addition, an internal oxide zone also consisting of the NiO-CoO solid solution develops within the alloy. In agreement with the analysis presented here, the amount of internal oxide decreases with the distance below the surface scale/alloy interface. Unfortunately, the only relevant analysis of the internal oxide is that of Stott [4] for Ni-20.6 and Ni-38.4 wt. percent Co alloys oxidized at 1100°C, and this will be used in a later comparison. Table IV summarizes Stott's data on the internal oxidation of these alloys. However, before making the comparison between these data and the quantitative predictions of the present analysis, it is necessary to consider briefly the growth and composition of the surface scale.

Interdiffusion in Ni-Co alloys is relatively slow in comparison with the growth of the surface scale. As a consequence of this [2], the overall ratio of Co to Ni in the surface scale is very close to that in the alloy. The scale is not, however, of uniform composition since Co^{++} ions have a higher diffusivity than Ni^{++} ions in the oxide solid solution and, as a consequence, Co tends to concentrate toward the outer part of the scale, leaving the scale adjacent to the alloy phase with a higher Ni content. These concentration profiles, which develop in the surface scale during oxidation, have been well-modeled by solving the appropriate diffusion equations [13], and show very good agreement with

experimentally determined profiles. In the present context, the important parameter is the scale composition at the surface scale/alloy interface, which is given under these conditions [14]:

$$\zeta'_{CoO} = pN_{Co}^{O}/(1-N_{Co}^{o}) + pN_{Co}^{o}$$

where ζ'_{CoO} is the equivalent fraction of Co at the alloy/scale interface, N_{Co}^{o} is the mole fraction of Co in the bulk alloy, and p is the ratio of self-diffusivities of Ni^{++} to Co^{++} ions in the oxide solid solution. Using the above equation and a value of p of 0.2, which represents an average of the somewhat scattered data available (see Ref. 13), the scale composition at the alloy/surface scale interface has been calculated for the two Ni-Co alloys referred to earlier--namely, Ni-20.6 wt. percent Co and Ni-38.4 wt. percent Co. The value for the latter alloy is shown on the phase diagram in Fig. 3 as point f. The oxygen activity at the alloy/surface scale interface is also fixed by the scale composition at point f, and because of the usual and reasonable accumption of local thermodynamic equilibrium between surface scale and alloy, the alloy composition is also fixed, point e. As indicated earlier, however, diffusion in the underlying alloy is very slow compared to the growth of the surface scale; and depletion in Co, the selectively oxidized element, will penetrate only a negligible distance into the alloy. In addition, the diffusion rate of oxygen

into the alloy is also considerably greater than the alloy interdiffusion coefficient: The limited data for oxygen diffusion in pure Ni indicate values of the diffusion coefficient in the range 6.3×10^{-8} to 1.3×10^{-6} cm^2/s at 100°C [15]. Thus, as indicated earlier, any overall change in the ratio of Co to Ni in the internal oxidation zone is unlikely, although the oxide phase will be enriched in Co, and the alloy phase correspondingly depleted. Thus, the overall ratio of metallic components averaged over oxide and alloy phases in the internal oxide zone remains equal to the ratio in the bulk alloy, and the diffusion path in the subscale zone adopts a right-angle shape.

As indicated in an earlier paper [1], it would be unrealistic for the right-angled portion of the diffusion path to contact point e, representing the alloy/surface scale directly, since it would then cut right across the two-phase alloy plus scale field and into the single-phase scale field (fedcba in Fig. 3). Therefore, there is a thin band of alloy phase, represented by ed, separating the surface scale from the subscale zone. The precise reason for this is not entirely clear, but is observed experimentally.

The exact location of point d, where the subscale zone commences, cannot be determined a priori unless the maximum fraction of subscale is known. In the present analysis it has been assumed that this is 0.3, in accord with Rapp's observations [16] that this is the critical volume fraction of internal oxide at which

transitions from exclusion internal oxidation to external scaling occurs.

One further assumption is necessary. The oxygen solubility in the Ni-Co alloys has not been determined. As a consequence, it has been necessary to assume that the Henrian activity coefficient for oxygen dissolution in the alloy is unity and independent of alloy composition. Thus, the atomic solubility of oxygen is given as

$$N_O = N_{CoO}/N_{Co} \exp [\Delta G^o_{CoO}/RT] .$$

Using the data included above and the experimentally determined rate constants for growth of the surface scale converted into rate constants K_1 which relate to the displacement of the alloy/surface scale interface (summarized in Table III), Eq. (16) was solved to give K_2, the rate of penetration of the front of internal oxidation. Then Eqs. (1), (2), (8), and (14) were solved to give the composition of the alloy, the composition of the internal oxide, the fraction of internal oxide, and the concentration of dissolved oxygen throughout the subscale zone.

The resulting profiles are shown in Figs. 4 and 5 for the Ni-10.9 and 38.7 wt. percent Co alloys, respectively, oxidized for 3 h at 1100°C. The depths of internal oxidation below the surface scale/alloy interface were 20 and 11 μm, respectively, for the two alloys; and the values of oxygen diffusivity used in the calculation

were adjusted to give similar subscale thicknesses. These values were 3.9×10^{-6} 3.7×10^{-6} cm^2/s for the two alloys, respectively. These values are consistent with one another but are on the high side of the independently measured values reported above. However, experimental determination of the depth of internal oxidation is made difficult by the irregular nature of both alloy/surface scale and alloy/internal oxide interfaces.

Included in Figs. 4 and 5 are the experimental analyses of the internal oxide composition of the two alloys. In both cases, agreement between experimental and calculated values is rather poor, although qualitatively both show the expected trend of an increasing concentration of Co in the internal oxide with increasing distance into the alloy. The reasons for these discrepancies may well lie in the tentative assumptions of the present analysis and the relatively unreliable data of diffusion coefficients and oxygen solubility. In addition, however, there are difficulties associated with precise analyses of the internal oxide particles due to overlapping effects of the x-ray source. The individual oxide particles in the Ni-Co systems, though, appear to be of 5-10 μm in size [4].

As indicated earlier, when the selectively oxidized component in the alloy is also the faster diffusing species in the oxide scale, as in the Ni-Co system, it appears from superimposing the diffusion path in the alloy-p_{O_2} diagram that there must be a region of alloy immediately below the scale that does not contain any subscale. This is not necessarily the case where the selectively

oxidized element is the slower diffusing species in the scale. The Co-Mn system is such a case in which Mn has the higher affinity for oxygen but Co^{++} diffuses faster in the (CoMn)O solid solution scale. However, the Co-Mn-O cannot be analyzed according to this treatment since the use of acceptable values for D_0 (presumably of the order of $5 \times 10^{-8} cm^2/s^{-1}$), the calculated value of $\partial r/\partial N_0$ of 8.8×10^5 and the experimental [18] value of K_1 of 6.8×10^{-10} cm^2/s for a Co-6.5 wt. percent Mn alloy leads to $\gamma_1 = 5.48$. With this rather large value of γ_1, Eq. (16) cannot be solved, due to the asymptotic properties of erfc that make it indistinguishable from zero for arguments greater than five. The calculation may be performed with much larger values of D_0 ($D_0 > 10^{-4}$ cm^2/s), leading to smaller values of γ_1, but this has no physical meaning. Therefore, because of these computational difficulties this treatment cannot produce significant results for this system, although this does not detract from its general applicability to these types of alloys.

An additional feature that may also be important is that the presence of subscale in the alloy can also enhance the diffusion of the alloying components. In particular, it has been seen that the transport of cations in the oxide can be an order of magnitude or more greater than transport in the alloy and, as a consequence, the internal oxide phase may act as a short-circuit path to enhance the enrichment of the more easily oxidizable component in the internal oxidation zone.

Conclusions

The diffusion processes occurring when binary alloys react with a simple oxidant to form an oxide that contains both alloy components in solid solution either exclusively as internal oxide or in combination with a surface scale have been analyzed and compared with experimental results for Fe-Mn and Ni-Co alloys. In the former case, the oxidizing conditions were such that only internal oxides were formed. The Mn concentration in the oxide phase increased with distance below the alloy surface, as does the Mn concentration in the alloy remaining in the internal oxide zone. There is good agreement between calculated and experimental values for these latter concentrations. In the Ni-Co system, a surface scale and a zone of internal oxide develop, both consisting of the NiO-CoO solid solution. Agreement between calculated and experimentally measured depths of internal penetration is acceptable if the diffusivity of oxygen in the alloy is about 3.8×10^{-6} cm^2/s at 1100°C. Agreement between calculated and experimental concentration profiles is not very good.

Acknowledgment

A portion of this work has been supported by the Division of Materials Science, Office of Basic Energy Sciences, U.S. Department of Energy under Contract No. W-7405-Eng-48.

Appendix

List of Principal Symbols

B	alloy component with higher affinity for oxygen
BO	more stable scale component
a_O	activity of oxygen
D_O	diffusivity of oxygen in the alloy
D_O^{eff}	effective diffusioin coefficient of oxygen in alloy
f	volume or mass fraction of internal oxide
f_{max}	maximum volume or mass fraction of internal oxide
ΔG^o_{AO} ΔG^o_{BO}	free energies of formation of oxides AO and BO, respectively
N_B	mole fraction of component B in the alloy
N_B^o	bulk mole fraction of component B in the alloy
N_{BO}	mole fraction of oxide BO in oxide phase
N_O	atomic fraction of oxygen dissolved in alloy
N_O^I N_O^{II}	atomic fraction of oxygen dissolved in alloy at the internal oxide/surface scale and alloy/internal oxide interfaces, respectively
R	gas constant
r	ratio of number of moles of precipitated oxide to total number of moles of metallic constituents in the alloy

T	temperature
t	time
X_1, X_2	positions of internal oxide/surface scale and internal oxide/alloy interfaces, respectively
x	position coordinate
β	defined as $[-1/RT\ \Delta G^{o}_{BO}]$
γ_1, γ_2	dimensionless rate constants describing rate of displacement of the internal oxide/surface scale and internal oxide/alloy interfaces, respectively
γ^{o}_{O}	Henry's law activity coefficient for oxygen dissolved in alloy
Ω	defined as $[-1/RT\ (\Delta G^{o}_{BO} - \Delta G^{o}_{AO})]$

Footnotes

1. D.P. Whittle, F. Gesmundo, B.D. Bastow, and G.C. Wood, Phil. Mag., to be published.
2. B.D. Bastow, D.P. Whittle, and G.C. Wood, Proc. Roy. Soc. A356 (1977) 177-214.
3. J.H. Swisher, Trans. Met. Soc., AIME 242 (1968) 205-209.
4. J.M. Ferguson and F.H. Stott, PhD theses, University of Manchester (1967,1970).
5. J.H. Swisher and E.T. Turkdogan, Trans. Met. Soc., AIME 239 (1967) 426-431.
6. C. Wells and R.F. Mehl, Trans. Met. Soc., AIME 145 (1941) 315-328.
7. J.F. Butler, C.L. McCabe and H.W. Paxton, Trns. Met. Soc., AIME 221 (1961) 479-484.
8. P. Roy and R. Hultgren, Trans. Met. Soc., AIME 233 (1965) 1811-1815.
9. K. Schwerdtfeger and A. Muan, Trans. Met. Soc., AIME 236 (1966) 201-208.
10. O. Kubachewski, E.L. Evans, and C.B. Alcock, "Metallurgical Thermodynamics," Pergamon Press, Oxford, England (1967).
11. E. Ankrust and A. Muan, Trans. Met. Soc., AIME 227 (1963) 1378.
12. R.J. Moore and J. White, J. Mater. Sci. 9 (1974) 1393.

13. B.B. Bastow, D.P. Whittle, and G.C. Wood, Corros. Sci. 16 (1976) 57.

14. D.P. Whittle, B.D. Bastow, and G.C. Wood, Oxid. Met. 9 (1975) 215.

15. Diffusion Data (1974).

16. A.A. Rapp, Corrosion 21 (1965) 382.

Table I. Thermodynamic and Solubility Data for the Fe-Mn-O System at 1350°C.

Ω	3.104×10^{3}
β	3.815×10^{8}
oxygen solubility ($P_{H_2O}/P_{H_2} = 0.2$)	5.57×10^{-4} wt.percent
oxygen solubility, atomic fraction	1.95×10^{-5}
oxygen potential ($P_{H_2O}/P_{H_2} = 0.2$)	1.72×10^{-6} $atm^{1/2}$
γ_O^O	8.82×10^{-2}

Table II. Calculated Internal Oxidation Parameters for Fe-1 % Mn Oxidized in $H_2O/H_2(0.2)$ at 1350°C.

r_I	= 0.0113
f_I	= 0.0112
N_{MnO}^I	= 0.789
N_{Mn}^I	= 0.001
N_O^I	= 1.95×10^{-5}
N_O^{II}	= 2.88×10^{-6}
N_{MnO}^{II}	= 0.969
γ_2	= 2.23
$\partial r/\partial N_O$	= 680
D_O^{eff}	= 2.79×10^{-8} cm^2/s

Table III. Thermodynamic and Solubility Data for the Ni-Co-O System at 1100°C.

		5.591	
β		1.6×10^{5}	
	Ni-20.9 wt. / CO		Ni-38.7 wt. / Co
N_{Co}^{o}	0.206		0.384
$N_{O}^{I(r=0.3)}$	2.22×10^{-5}		1.46×10^{-5}
K_1, cm^2/s	1.25×10^{-10}		3.07×10^{-10}
D_O, cm^2/s	3.9×10^{-6}		3.7×10^{-6}

Table IV. Experimental [4] Internal Oxidation Date for Ni-Co Alloys Oxidized 3 h at 1100°C.

	Ni-20.9 wt. / Co			Ni-38.7 wt. / Co		
Surface scale thickness, μm	25-28			43-45		
Subscale thickness, μm	18-22			9-13		
N_{CoO} as a function of depth below the alloy/ surface scale interface	wt. / Co	N_{CoO}	μm	wt. / Co	N_{CoO}	μm
	28.5	0.365	5	39.0	0.497	2
	31.0	0.392	9.5	41.1	0.525	5
	32.7	0.415	20	43.0	0.549	7

Figure Captions

Fig. 1. Calculated and experimental [3] concentration profiles through the subscale formed on Fe-1 percent Mn during oxidation at 1350°C in $H_2O/H_2(0.2)$ atmospheres.

Fig. 2. Comparison of N_O/N_{Mn} ratio as a function of position in the subscale according to present analysis and that due to Swisher [3].

Fig. 3. Ni-Co-$P_{O_2}^2$ diagram showing diffusion path through subscale zone for Ni-20.9 wt percent Co.

Fig. 4. Calculated and experimental [4] concentration profiles through the subscale for Ni-10.9 wt. percent Co oxidized at 1100°C for 3 h.

Fig. 5 Calculated and experimental [4] concentration profiles through the subscale for Ni-38-8 wt. percent Co oxidized at 1100°C for 3 h.

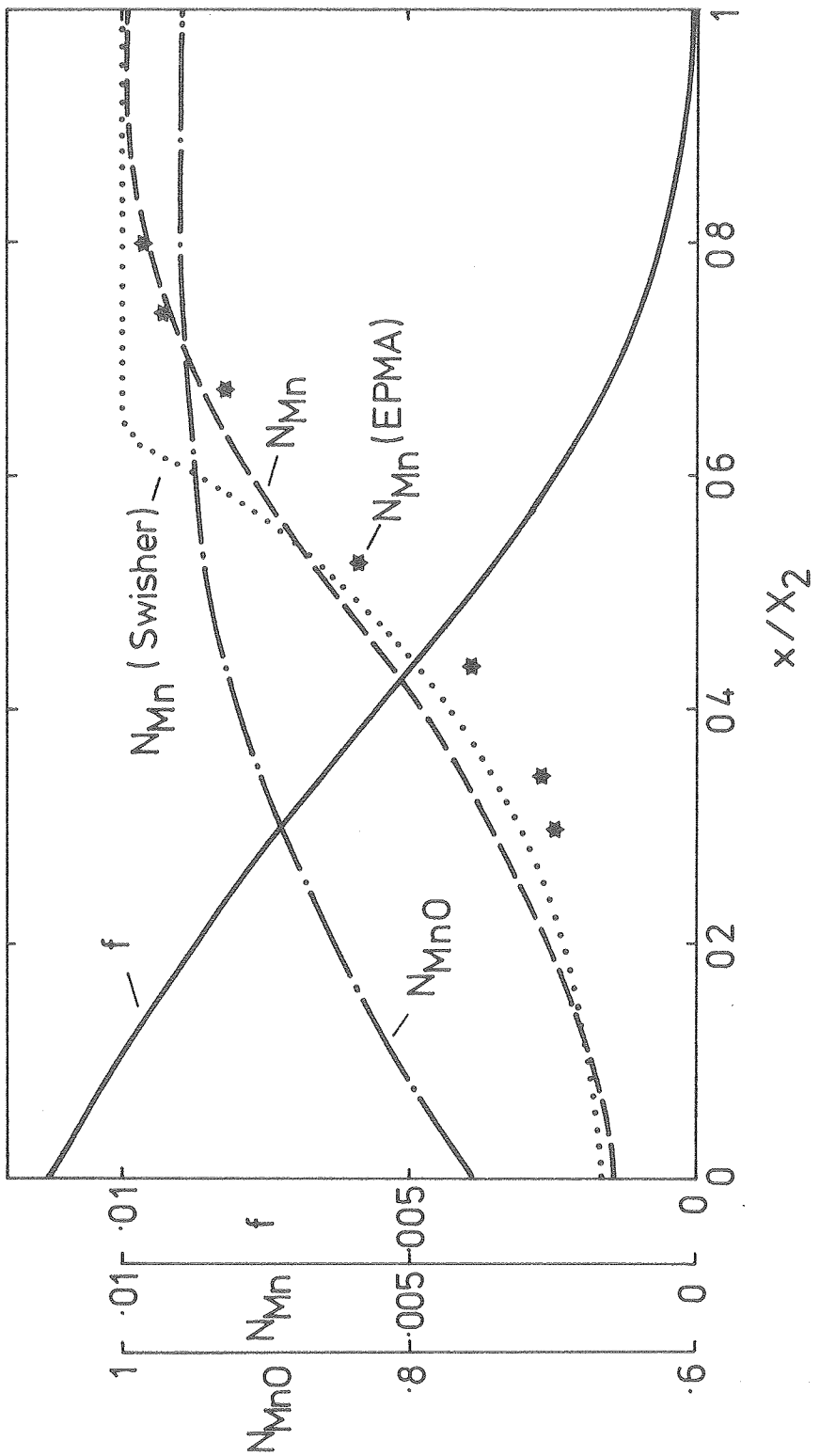

XBL 809-11864

Figure 1

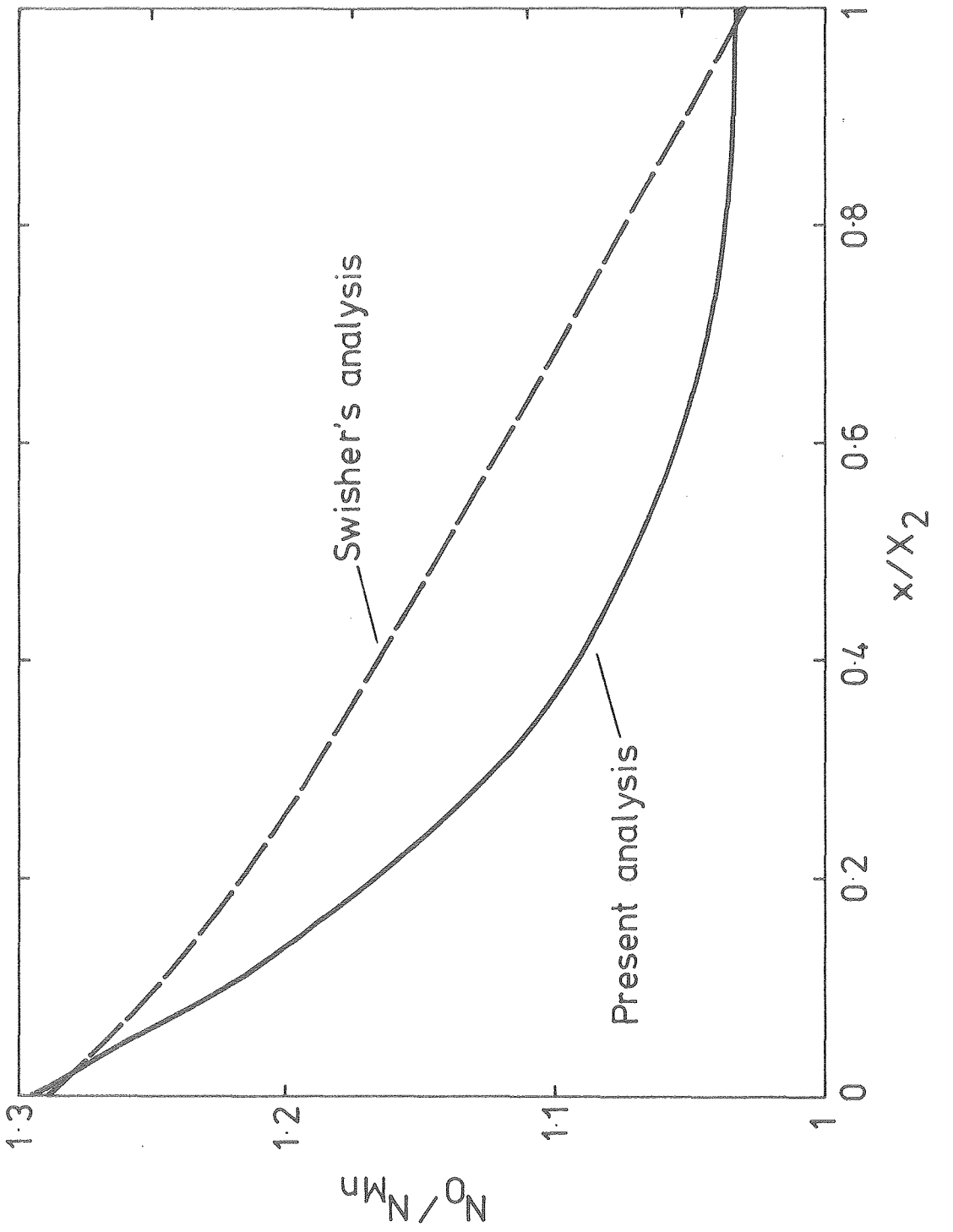

XBL 809-11867

Figure 2

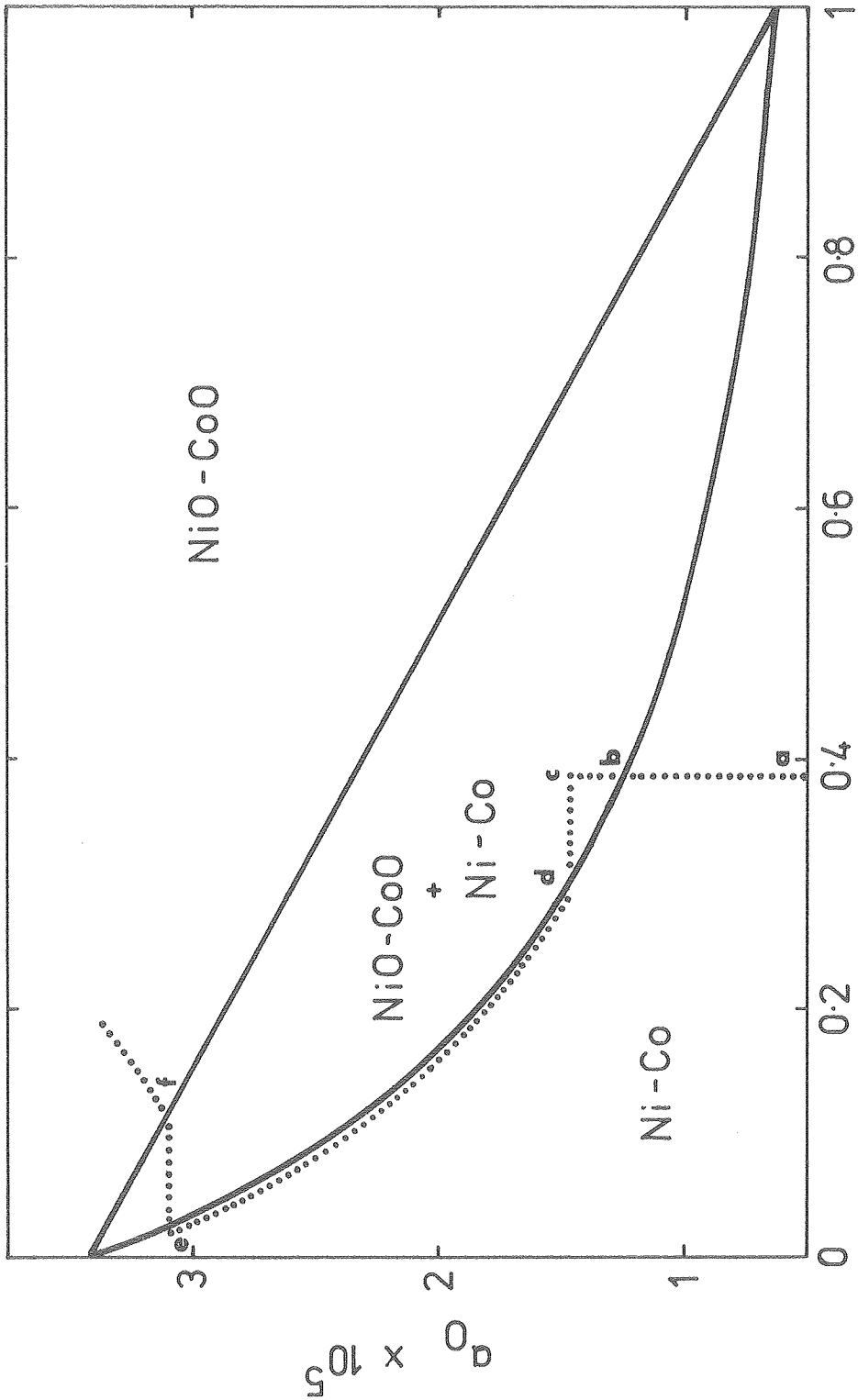

XBL 809-11863

Figure 3

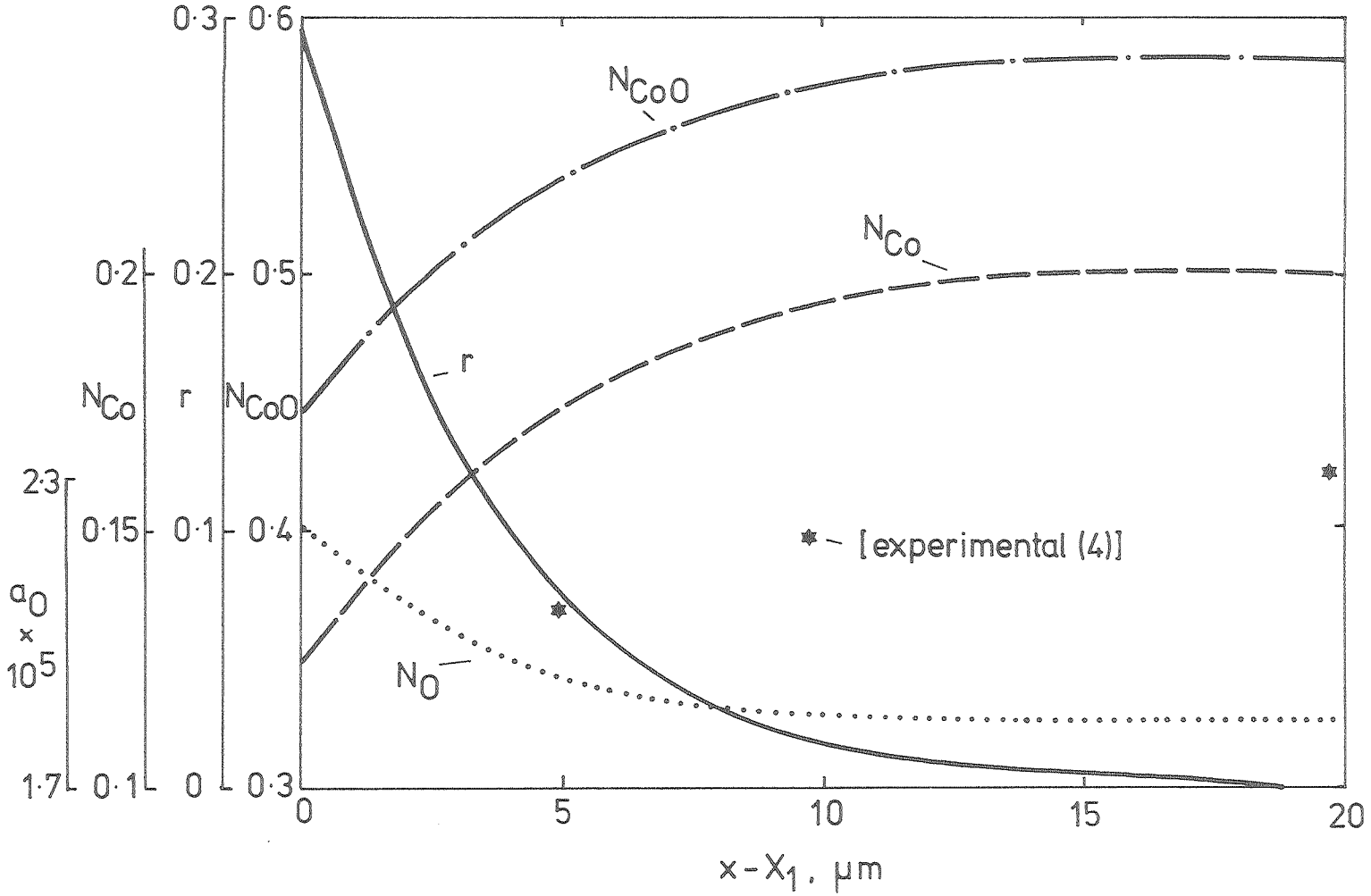

XBL 809-11866

Figure 4

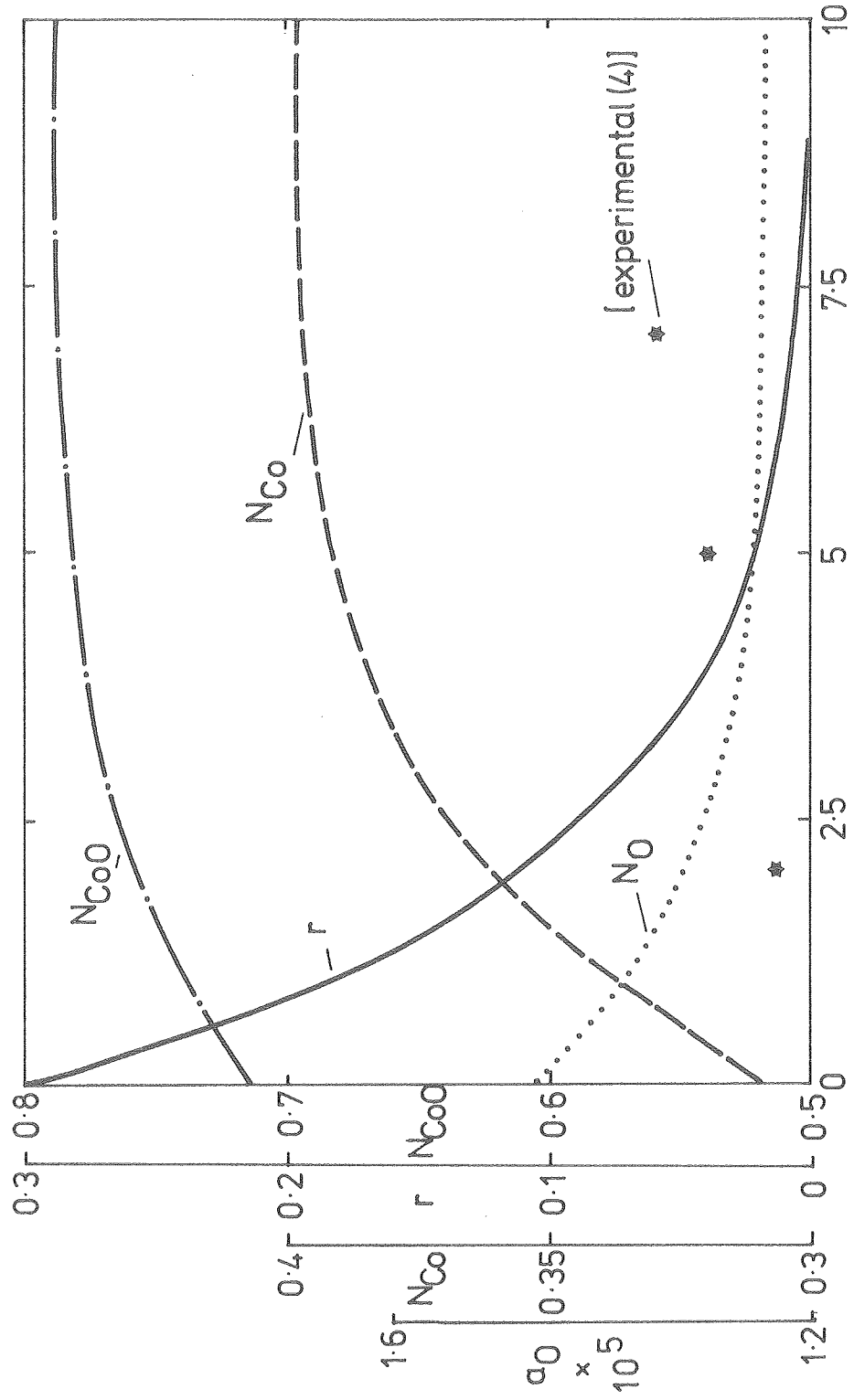

XBL 809-11865

Figure 5